# A Neural Mass Computational Framework to Study Synaptic Mechanisms Underlying Alpha and Theta Rhythms

**Basabdatta Sen Bhattacharya and Simon J. Durrant**

## Introduction

Building biologically-inspired computational tools is gaining in popularity for advancing neuroscience research towards understanding and predicting neurological and psychiatric disorders [6, 16]. However, computational time and resources have been a major challenge towards such endeavours. Population-level representations (as opposed to networks of single neuronal models) that can simulate higher-level brain dynamics observed in Electroencephalogram (EEG) and Local Field Potentials (LFP) can address the computational constraints to a fair extent, for example neural mass models [21, 53, 54]. The term 'neural mass' was coined by Walter J. Freeman [32] to define the collective behaviour of a mesoscopic scale neuronal population ($\approx 10^4$–$10^7$ neurons) that are packed densely in a spatial area of 0.3–3 mm and may be assumed as a single entity [48]; Freeman's work comprised neuronal behaviour and dynamics in the olfactory pathway. Around the same time, Wilson and Cowan proposed the mathematical framework for modelling feed-forward and -back connections between excitatory and inhibitory 'point-neurons' (an ensemble representation of a neuronal population, along the lines of neural mass) that could mimic brain dynamics such as seen in EEG and LFP [75]. This mathematical framework forms the basis of a seminal work by daSilva [19] and Zetterberg et al. [76], where they introduced a block-diagram-like approach (from Control Engineering) to model a simple thalamocortical circuitry of the visual pathway for simulating alpha rhythms—oscillatory activity within 8–13 Hz seen in LFP and EEG record-

B. Sen Bhattacharya (✉)
University of Lincoln, INB 3225, Engineering Hub, Brayford Pool,
Lincoln LN6 7TS, UK
e-mail: basab.sen.b@gmail.com

S.J. Durrant
School of Psychology, University of Lincoln, Brayford Pool, Lincoln LN6 7TS, UK
e-mail: sidurrant@lincoln.ac.uk



P. Érdi et al. (eds.), *Computational Neurology and Psychiatry*,
Springer Series in Bio-/Neuroinformatics 6,
DOI 10.1007/978-3-319-49959-8_14

ings. The interaction between thalamic and cortical networks are now well known to underlie brain oscillatory patterns, referred to commonly as 'brain rhythms' [14], corresponding to cognition, perception and sleep-wake transitions [45, 65]. Subsequently, Lopes da Silva's thalamocortical neural mass model mimicking alpha rhythm was further extended in [43, 66, 74]; these works set a 'trend' of adopting neural mass models of thalamocortical circuitry in clinical neuroscience research towards mimicking brain rhythms of both health and disease conditions [13, 37, 55, 63, 67, 70] (see [22] for a review).

Alpha rhythms are traditionally believed to represent an idling state of the brain and is most prominent in EEG from occipital scalp (the seat of visual cortex) when a subject is awake and resting with eyes closed; the rhythms subside when the eyes are opened. However, in current times and with advancing research, it has emerged that the alpha rhythms also play an integral role in various awake cognitive states [50]. Furthermore, alpha to theta (4–7 Hz) shift is an EEG marker of brain state transition from quiet wakefulness (preceding sleep) to a state of drowsiness (sleep stage-I). At the same time, anomalies of alpha rhythmic oscillations are indicators of several disease conditions, for example 'slowing' (reduced frequency of peak power) of the alpha rhythm is a hallmark of EEG in Alzheimer's disease [8, 44]. Similarly, thalamocortical dysrhythmia (TCD), a shift of peak frequency from alpha to theta, is an EEG marker of several disorders such as Tinnitus, Neurogenic Pain, Depression [41, 49, 60]. We have proposed a modification to the alpha rhythm model in [19] to show a significant effect of reduced synaptic connectivity from inhibitory cell populations in simulating AD related conditions in the model [8]. This is consistent with autopsy studies in AD showing impaired inhibitory pathways [31]. However, a major constraint in the classic neural mass computational models is the use of Ralls alpha function [56]; although the alpha function is a fair estimation of the synaptic transmission process [4], it falls short when investigating disease conditions, where attributes such as transmitter concentration and ion-channel states might play a significant role. More recent research have used parameters from an experimental study [36] on a thalamic slice from mammal to model receptor dynamics during synaptic transfer in a neural mass model [67]. Along these lines, another biologically plausible alternative for modelling ligand-gated and secondary-messenger-gated synaptic transmission is to implement kinetic models [24, 25], which takes into account the transmitter concentration in the synaptic cleft and subsequent state of channels involved in generating the post-synaptic potential. Discussing the future benefits of kinetic modelling of synaptic processes, the authors in [23] reflect thus: "A considerable amount of experimental data is available from measurements of the average activity of populations of brain cells: recordings of electroencephalogram, local field potentials, magnetoencephalograms, optical recordings, magnetic resonance images, etc. It would be interesting to attempt to establish a relationship between such global measurements and dynamics at the molecular level". Indeed, such an approach was already adopted by Aradi and Erdi [2] and Erdi et al. [30] in network models of hippocampal neurons to investigate neuropharmacological solutions to neuro-psychiatric disorders.

In prior works, a novel approach is adopted for classic neural mass models where Rall's alpha function is replaced by kinetic models of Glutamatergic and $\gamma$-amino-butyric-acid (GABA)-ergic synapses mediated by $\alpha$-amino-3-hydroxy-5-methyl-4-isoxazolepropionic-acid (AMPA) and $GABA_{A,B}$ neuroreceptors respectively [5, 10]. The motivation for these works have been to take a step forward in building computational tools that can complement experimental research in understanding the underlying cellular mechanisms of anomalous EEG signals in neurological and psychiatric disorders. In addition, this novel approach reduces the computational time by an order of 10 compared to the classic neural mass model for similar thalamocortical structures. Implementing this approach for a thalamocortical model have demonstrated model sensitivity to neurotransmitter concentration, forward and reverse rates of reaction and leak conductance in the model in effecting change in time-series patterns as well as shifting the power spectrum [5].

In this work, we present a thalamocortical model representing the three neuronal population of the Lateral Geniculate Nucleus (LGN) viz. the thalamocortical relay (TCR) neurons that are the main carriers of sensory information to the cortex; the thalamic interneurons (IN); the thalamic reticular nucleus (TRN) that receive a 'copy' of all information transfer between the TCR and the cortex [61]. The synaptic layout of the model is based on data obtained from LGNd (dorsal) slices of cat and rat thalamus [40, 45, 62]. Each parameter corresponding to synaptic attributes in the model is a representation of the population average of the parameter value in the respective neural mass. The AMPA and $GABA_A$ synapses in the model are simulated by two-state kinetic models. In the visual pathway, simultaneous LFP and EEG recordings from the TCR cells (thalamus) and the cortex respectively show a high degree of correlation [17, 20]. Thus, the output from the TCR population in the model is assumed to be a simulation of LFP recordings from LGN. We assume a de-corticated LGN (thalamus), similar to an approach adopted in early experimental works [3, 46, 51, 52, 64] looking into independent thalamic cell behaviour, which allowed an in-depth understanding of the thalamus as a key player in generating and sustaining brain oscillations. These pioneering works on LGN slices in vitro showed that the thalamus is capable of displaying oscillations even in a de-corticated state, and that similar thalamic mechanisms underlie alpha and theta rhythms of EEG and LFP [42]. The results from our model conform to these experimental observations and identify the neurotransmitter concentration in the synaptic cleft as a crucial parameter that impact transition between alpha and theta oscillatory dynamics. In addition, our results indicate distinct inhibitory roles for the IN and the TRN population, the former acting as a 'balancing' element in the circuit, the latter taking a dominant role in effecting (spindle-like) 'waxing-and-waning' and limit cycle oscillations.

In section "A Kinetic Model Based Framework for Neural Mass Modelling of the Thalamic Circuit", we present an overview of kinetic modelling of AMPA and $GABA_A$ based neuroreceptors in context to their embedding in the neural mass models. This is followed by a description of the neural mass model of LGN presented in this work. The results of model simulation are demonstrated in section "Results and Discussion" and their implications are discussed. We conclude in section

"Conclusion" with a recapitulation of the salient observations made in section "Results and Discussion" and a discussion of ongoing and future work.

## A Kinetic Model Based Framework for Neural Mass Modelling of the Thalamic Circuit

A simple mathematical model defining the chemical kinetics of ion-channel is proposed in [24] as a computationally efficient means of studying detailed synaptic attributes in neuronal models. The dynamics of each ion channel is represented by

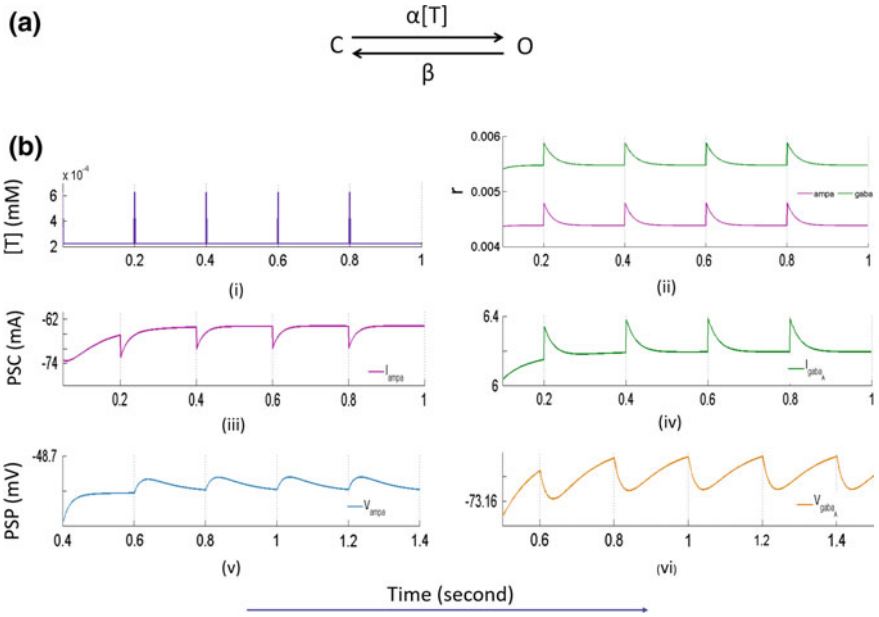


**Fig. 1** **a** The state transition diagrams for AMPA and $GABA_A$ neuroreceptor dynamics defined in Eq. (1); $\alpha$ and $\beta$ are rate of transitions between the two states; The desensitised state of the ion-channels are ignored in this work for brevity (see [25] for a detailed comparison of kinetic models simulating more than two-states). **b** The response function $[T]$ corresponding to an impulse train of magnitude 2 mV and a base voltage of −65 mV applied at an arbitrarily selected rate of 4 Hz is shown in panel (i). (The readers may note that for the purposes of this work, all parameters in Eq. (2) are same for both AMPA and $GABA_A$ mediated synapses. Thus, any change in the equation parameters result in a change in $[T]$ in all synaptic junctions of the model). Panel (ii) shows the corresponding change in proportion of open ion channels ($r$). Panels (iii) and (v) show the negative post synaptic membrane current (PSC) and the positive (excitatory) post synaptic membrane potential (PSP) corresponding to the AMPA neuroreceptor mediated synapses. Conversely, a positive PSC and a negative (inhibitory) PSP is shown for $GABA_A$ mediated synapses in panels (iv) and (vi) respectively

two states as shown in Fig. 1a: an unbound state referred to as 'C' denoting the closed state of the ion channels; a bound state referred to as 'O' denoting open states of the same. While the 'two-state' model is an abstracted representation of complex ion-channel dynamics, it is reported to be a fair approximation of the higher state models [25]. In the following sections, we present the two-state kinetic model of ion channels in the post-synaptic neuronal membrane responding to AMPA and $GABA_A$ neuroreceptor based signal transmission, which are then implemented in a neural mass model of the LGN to simulate LFP dynamics.

## *AMPA and $GABA_A$ Based Neurotransmission*

The proportion of open ion channels on the post-synaptic cell membrane ($Y$) corresponding to the synapse mediated by the neurotransmitter receptor $\bar{\eta} \in \{AMPA, GABA_A\}$ is represented by $r_Y^{\bar{\eta}}$, and the two state dynamics are defined in Eq. (1):

$$\frac{dr_Y^{\bar{\eta}}(t)}{dt} = \alpha^{\bar{\eta}}[T]_\chi(1 - r_Y^{\bar{\eta}}(t)) - \beta^{\bar{\eta}} r_Y^{\bar{\eta}}(t) \tag{1}$$

where $\alpha^{\bar{\eta}}$ and $\beta^{\bar{\eta}}$ are the rate transitions from the open to the closed state and vice-versa respectively and corresponding to the synapses mediated by $\bar{\eta}$. Furthermore, $r_Y^{\bar{\eta}}$ is a function of the concentration of neurotransmitters in the synaptic cleft ($[T]_\chi$), which in turn is a function of the pre-synaptic cell ($\chi$) membrane potential ($V_\chi$) and is approximated as a sigmoid function shown in Eq. (2).

$$[T]_\chi(V_\chi(t)) = \frac{T_{max}}{1 + exp\,(-\frac{V_\chi(t) - V_{thr}}{\sigma})} \tag{2}$$

$T_{max}$ is the maximum neurotransmitter concentration and is well approximated by 1 mM (milliMole) [23]. The parameter $V_{thr}$ represent the threshold at which $[T]_\chi = 0.5T_{max}$ while $\sigma$ affects the steepness of the sigmoid. The resulting post-synaptic current (PSC) is defined in Eq. (3):

$$I_Y^{\bar{\eta}}(t) = g^{\bar{\eta}} r_Y^{\bar{\eta}}(t)(V_Y^{\bar{\eta}}(t) - E^{\bar{\eta}}) \tag{3}$$

where $g^{\bar{\eta}}$ and $E^{\bar{\eta}}$ are the maximum conductance and membrane reversal potential respectively of the post-synaptic cell corresponding to the $\bar{\eta}$ mediated synapse; $V_Y^{\bar{\eta}}$ is the post synaptic membrane potential (PSP) corresponding to the $\bar{\eta}$-mediated synapse, and is defined in Eq. (4):

$$V_Y^{\bar{\eta}}(t) = \frac{1}{\kappa_m} \int I_Y^{\bar{\eta}}(t)\, dt, \tag{4}$$

**Table 1** The range of parameter values are referred from [9, 24, 36, 67, 71]. The exact parameter values in the model are set by trial simulations such that the model output time-series has a dominant frequency within the alpha band (8–13 Hz). (A) Data for the forward ($\alpha$) and reverse ($\beta$) rates of synaptic transmission is according to the range mentioned in [24, 36]. Note that the units used in our model is at a different time scale ($sec^{-1}$), and thus absolute figures are different from these references. The data for maximal synaptic conductance $g^{\bar{\eta}}$ is in the range mentioned in [36, 71]; note that the unit for this parameter in our model is $\mu S/cm^2$. Data for $E^{\bar{\eta}}$ is as in [36, 71]. Specific data relating to the thalamic IN synapses are not mentioned in any of these sources, and are set as similar to those of TRN in this work. The 'RET' in the parameter superscripts refer to the retina as the source of input to the model. (B) The leakage current in the model cell populations are assumed to be due to Potassium (K) mainly. Thus, the leakage conductance and reverse potentials parameters in the model are in the range mentioned in [36, 71]. The resting state membrane potential for TCR and TRN are as in [71]; the resting state membrane potential for IN is set arbitrarily at a hyperpolarised value with respect to that of the TCR. The resting membrane potential for RET is set at −65 mV, and is simulated by a random white noise with mean −65 mV and standard deviation 2 $mV^2$. This signal represents the mean membrane voltage of the retina as an afferent to the TCR cell populations. Thus, there is no ODE corresponding to the RET in the model, and its leak conductance and leak reversal potentials are indicated with '*X*'

(A) Neurotransmission parameters

| Parameters | Value | Synaptic pathway |
|---|---|---|
| $\alpha$ $\left((\text{mM})^{-1}\cdot(\text{s})^{-1}\right)$ | 1000 | AMPA, $GABA_A$ |
| $\beta$ ($s^{-1}$) | 50 | AMPA |
| | 40 | $GABA_A$ |
| $g^{\bar{\eta}}$ ($\mu S/cm^2$) | 300 | AMPA (RET to TCR) |
| | 100 | AMPA (RET to IN) (TCR to TRN) |
| | 100 | $GABA_A$ |
| $E^{\bar{\eta}}$ (mV) | 0 | AMPA |
| | −85 | $GABA_A$ (TRN/IN to TCR) |
| | −75 | $GABA_A$ (TRN (IN) to TRN (IN)) |

*(B) Cell membrane parameters*

| | RET | TCR | IN | TRN |
|---|---|---|---|---|
| $g^{leak}$ ($\mu S/cm^2$) | X | 10 | 10 | 10 |
| $E^{leak}$ (mV) | X | −55 | −72.5 | −72.5 |
| $V_{rest}$ (mV) | −65 | −65 | −75 | −85 |

where $\kappa_m$ is the post-synaptic membrane capacitance. The input $V_\chi$ is an impulse train of amplitude 2 mV at a base value of −65 mV and at an arbitrarily selected rate of 4 Hz. The resulting neurotransmitter concentration $[T]_\chi$, probability of opening of ion channel $r_Y^{\bar{\eta}}$, PSC ($I_Y^{\bar{\eta}}$) and PSP ($V_Y^{\bar{\eta}}$) are shown in Fig. 1b; all parameters used for generating Fig. 1b are as mentioned in Table 1(A).

In the following section, we present a neural mass model of the thalamic circuitry where the excitatory and inhibitory alpha functions are replaced with two-state kinetic models of AMPA and $GABA_A$ mediated synapses respectively as defined in Eqs. (1)–(4).

## *A Neural Mass Model of the Lateral Geniculate Nucleus Implementing Synaptic Kinetics*

Experimental research on the Lateral Geniculate Nucleus (LGN) of mammals and rodents suggest two basic cell types: the thalamocortical relay (TCR) cells and the interneurons (IN). In addition, the thalamus is surrounded by a thin sheet of cells that receive copies of both afferent and efferent communication between thalamus and the cortex; this group of cells is considered as a part of the thalamus and is called the thalamic reticular nucleus (TRN). The neural mass model presented in this work is based on the synaptic layout of the LGN and is shown in Fig. 2. In addition to the fast excitatory (AMPA) and inhibitory ($GABA_A$) synapses in the LGN cell populations, the TRN also makes a slow inhibitory synapse on the TCR cells mediated by $GABA_B$ neuroreceptors [38]. However, in a previous study, the kinetic model of the $GABA_B$ synapse did not show any significant effect on the thalamocortical model output. Thus, this pathway is ignored in the current work (and is being investigated as a part of an ongoing work on the model). Also, while a feedback from the TCR to the IN cell

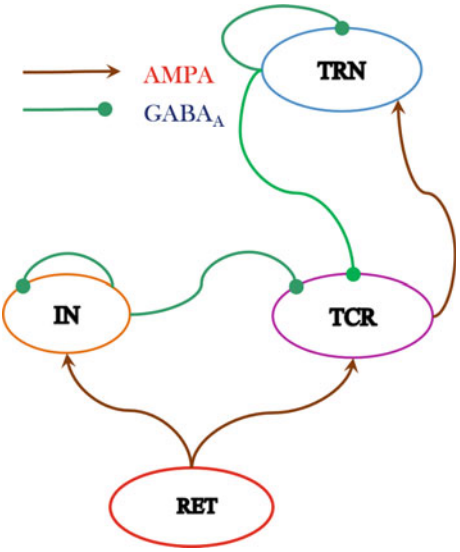


**Fig. 2** The synaptic layout of the model is based on experimental data obtained from the dorsal Lateral Geniculate Nucleus (LGNd) of mammals and rodents. Both TCR and IN cell populations of the LGN receive excitatory Glutamatergic inputs from the retinal spiking neurons (RET) that are mediated by AMPA neuroreceptors. The IN cell populations make a $GABA_A$ receptor mediated inhibitory synapse on themselves as well as on the TCR population. Information on the synaptic pathway from the TCR to IN is ambiguous in literature and is ignored in the current work. The TCR population make AMPA mediated excitatory synapses on the TRN population, while the TRN population make $GABA_A$ mediated inhibitory synapses on the TCR population as well as on itself. All synaptic connectivity parameter values in the model are derived from experimental data presented in [40, 45] and are mentioned in Table 2

population is suggested based on extrapolations from EEG-based studies [18, 77], the biological plausibility of this pathway is yet to be confirmed from experimental studies to the best of our knowledge. Thus, this pathway is ignored in the current model (as in our previous works [9, 11, 16]).

The underlying mathematical framework for the neural mass model implementing synaptic kinetics (Fig. 1a) is defined in Eqs. (5)–(9). The input to the model is assumed to be the ensemble membrane potential of pre-synaptic retinal cell populations ($V_{ret}$) in a resting state with no sensory input and is simulated using a Gaussian white noise [20] with a biologically plausible mean value of −65 mV. The standard deviation of the noise is set by trial and error to 2 $mV^2$ to reduce stiffness of the differential equations. All variables and parameters defined in the equations below are assumed to be the 'ensemble representation' corresponding to a neural mass; this is similar to the concept of a 'point neuron' representation of a localised neuronal population acting in synchrony. The output of the TCR population, hereafter referred to as the 'model output', is considered as the simulation of LFP dynamics recorded from LGN in mammals and rodents (for example from dogs in [19]).

$$[T]_{\bar{\chi}}(V_{\bar{\chi}}(t)) = \frac{T_{max}}{1 + exp(-\frac{V_{\bar{\chi}}(t) - V_{thr}}{\sigma})} \tag{5}$$

$$\frac{dr_{\bar{Y}}^{\bar{\eta}}(t)}{dt} = \alpha^{\bar{\eta}} \cdot [T]_{\bar{\chi}}(V_{\bar{\chi}}(t)) \cdot (1 - r_{\bar{Y}}^{\bar{\eta}}(t)) - \beta^{\bar{\eta}} \cdot r_{\bar{Y}}^{\bar{\eta}}(t) \tag{6}$$

$$I_{\bar{Y}}^{\bar{\eta}}(t) = g^{\bar{\eta}} \cdot r_{\bar{Y}}^{\bar{\eta}}(t) \cdot (V_{\bar{Y}}(t) - E^{\bar{\eta}}) \cdot C_{conn} \tag{7}$$

$$\kappa_m \frac{dV_{\bar{Y}}(t)}{dt} = - \sum_{\bar{Y} \in \{TCR, IN, TRN\}} (I_{\bar{Y}}^{\bar{\eta}}(t) + I_{\bar{Y}}^{leak}(t)), \tag{8}$$

$$I_{\bar{Y}}^{leak}(t) = g_{\bar{Y}}^{leak}(V_{\bar{Y}}(t) - E^{leak}), \tag{9}$$

where $\bar{\chi} \in \{RET, TCR, IN, TRN\}$ represent the pre-synaptic cell populations; $\bar{Y} \in \{TCR, IN, TRN\}$ represent the post-synaptic cell populations. The variables and parameters in Eqs. (5)–(8) are similar to those defined in Eqs. (1)–(4) and mentioned in Table 1(A). The normalised synaptic connectivity parameter $C_{conn}$ in Eq. (7) represent the collective 'fan-in' of synapses from a pre-synaptic population on to the post-synaptic population dendrites. Specific connectivity parameters in each synaptic pathway of the model shown in Fig. 2 is denoted as $C_{\bar{u}\bar{v}\bar{w}}$; see the legend of Table 2 for further details. All synaptic connectivity parameter values are obtained from literature on experimental data, for example in the TCR population, experimental studies on a sample population of cells indicate that approximately 7.1 % of the total number of incoming synapses are from the retinal ganglion cells, while 30.9 % of the synapses are from inhibitory cell populations. However, to the best of our knowledge, a quantitative distinction between the inhibitory inputs from the TRN and IN populations on to the TCR is not yet available. Thus, we have set the inhibitory connectivity parameter values for TCR afferents to an arbitrarily selected proportion of

**Table 2** Base values of the synaptic connectivity parameters $C_{conn}$ in Eq. (7) and derived from experimental data on LGNd of mammals and rodents [40, 45, 62] (as in our previous works [9, 16]). The nomenclature for the specific connectivity parameter in each synaptic pathway is $C_{\bar{u}\bar{v}\bar{w}}$: each parameter value in the table is a normalised figure that represents the percentage of the synaptic contacts made on the post-synaptic cell population $u$ by the pre-synaptic cell population $v$, and $w$ represents the nature of the synapse i.e. excitatory ($e$) or inhibitory ($i$). The model neuronal populations are represented by the letters $t$ for TCR, $n$ for TRN, $i$ for IN and $r$ for retina. For synaptic contacts by a cell population on itself, $v$ is represented by $s$, which stands for a connection from 'self'. All '$X$' indicate a lack of biological evidence for any synaptic connectivity in the specific pathway

| Efferents → Afferents ↓ | TCR | IN | TRN | Retinal |
|---|---|---|---|---|
| TCR | X | $C_{tii}$ $\frac{5}{8}$ of 30.9 | $C^{a}_{tni}$ $\frac{3}{8}$ of 30.9 | $C_{tre}$ 7.1 |
| IN | X | $C_{isi}$ 23.6 | X | $C_{ire}$ 47.4 |
| TRN | $C_{nte}$ 35 | X | $C_{nsi}$ 20 | X |

62.5($IN$) : 37.5($TRN$) in the model.[1] A similar abstraction is followed for parameterising the synaptic connectivity in the remaining model pathways and are mentioned in Table 2. While there is variation in reported data for the connectivity in literature on experimental studies, we follow the data specified in [40, 45]. The parameter $I^{leak}_{\bar{Y}}$ in Eq. (8) is the ensemble leak current of the post-synaptic population membrane defined in Eq. (9), where $g^{leak}_{\bar{Y}}$ and $E^{leak}$ are the maximum leak conductance and leak reversal potential respectively of the post-synaptic cell population $\bar{Y}$. The leak parameters as well as the resting membrane potentials for the model cell populations are mentioned in Table 1(B).

## *Empirical Methods*

The ODEs in Eqs. (5)–(9) are solved using the 4th/5th order Runge-Kutta-Fehlberg method (RKF45) in Matlab for a total duration of 40 s at a resolution of 1 ms. The output voltage time-series is averaged over 20 simulations, where each simulation

[1] In previous works with $GABA_B$ pathway from the TRN to the TCR, we have maintained an equal proportion of fan-in on the TCR from the IN and TRN. Thus, total synaptic contact from TRN to TCR has been $\frac{1}{2}$ of 30.9 %. Now, TRN makes both $GABA_A$ and $GABA_B$ contact on the TCR; thus the proportionality of $GABA_A$: $GABA_B$ was maintained at 3 : 1, as the $GABA_B$ pathway showed minimal effect on the model. Here, we have ignored the $GABA_B$ pathway and diverted the proportion of connectivities in this pathway i.e. $\frac{1}{8}$ of 30.9 % to the $GABA_A$ pathway from the IN to the TCR. A combinatorial study on the possible proportionates in the $GABA_A$ pathway in the model remains to be explored in ongoing and future works.

runs with a different seed for the noisy input. For frequency analysis, a 30 s epoch (from 9–39 s) of the output signal from each of the 20 simulations is bandpass filtered between 1–100 Hz with a Butterworth filter of order 10. A 4-point Fast Fourier Transform (FFT) at a sampling frequency of 1000 Hz is applied to each of these filtered signals. The power spectral density (psd) is derived using the Welch periodogram with a Hamming window of segment length spanning 500 data points (half the size as that of the sampling frequency) and with overlap of 50 %. All of the 20 psd thus obtained are then averaged for further analysis. The bar plots show the mean power within the frequency bands theta (4–7 Hz) and alpha (8–13 Hz).

## Results and Discussion

The objective is to mimic the EEG corresponding to the state of 'quiet wakefulness' (i.e. when a subject is in an awake resting state with eyes closed, for example just before transition to a state of sleep) in the model output with a dominant frequency within the alpha band. The model input is simulated with a random white noise, representing the pre-synaptic mean membrane potential $V_{\bar{\chi}}$ producing low-level background firing in the retinal spiking neurons in a state of quiet wakefulness and no sensory input. This state of the model is taken as the 'base' state, and the corresponding set of model parameter values are referred to as 'base values'. All parameter variations in the model are carried out with respect to these base values to study the synaptic correlates of EEG band power alterations in both healthy (e.g. sleep-wake transition) and disease states. The results are presented in the following sections along with discussion on their implications in context to alpha and theta rhythms in the LGN.

### *The Causality of Neurotransmitter Concentration*

Presynaptic membranes are rich in a diverse range of potassium channels that are likely relevant to the fine-tuning and regulation of neurotransmitter release [28]. While membrane-derived lipids such as arachidonic acid can act to inhibit presynaptic potassium channels [15], it is reported that Na+/K+-ATPase is involved in the maintenance of the synaptic vesicles filled with transmitters to be released [68]. On the other hand, release of neurotransmitters is well known to be mediated by calcium ion-channel dynamics in the pre-synaptic membrane [17, 39]. However, and to the best of our knowledge, there is a lack of experimental data establishing a correlation between brain states and neurotransmitter concentration and/or rate of release in the synaptic cleft. Here, we use the neural mass computational framework to look into this aspect.

We speculate that the exact amount of neurotransmitter released in clefts is bound to be varying in time corresponding to varying brain states. We simulate this in the

model by varying specific parameters, at the same time identifying a set of base parameter values defining the neurotransmitter concentration levels such that the dominant power in the model output is within the alpha frequency band.

### Selecting Base Parameter Values

In Eq. (5), an increase in the steepness parameter $\sigma$ leads to a decrease in gradient of the sigmoid representing the amount of transmitter released for a given change in the pre-synaptic population mean membrane potential $V_{\chi}$. On the other hand, a decrease in the threshold voltage $V_{thr}$ effect an increase in the release of neurotransmitter into the synaptic cleft. A simultaneous variation of $V_{thr}$ and $\sigma$ is done to observe the correlation between neurotransmitter concentration $[T]$ and the region of alpha band dominance in the power spectra of the post-synaptic population average membrane potential $V_{\bar{Y}}$.

The readers may note that in the model, the parameters $V_{thr}$ and $\sigma$ are set as equal for both AMPA or $GABA_A$ mediated synapses. Thus, any variation of these parameters will result in a variation of neurotransmitter concentration in all the synaptic clefts in the model. This may be thought to be analogous to an 'overall system slow down' during reduced cognitive states such as falling asleep. A separate study on neurotransmitter concentration levels for AMPA and GABA mediated synapses will be carried out in future versions of the model. The results are shown in Fig. 3a–d.

Figure 3a and b show the inverse relation between $[T]$ and the model output $V_{TCR}$, indicating a dominant GABA-ergic influence on the TCR from both IN and TRN cell populations. The corresponding peak power plot in Fig. 3d shows a higher power content for depolarised output values in Fig. 3b and is mainly due to the increasing power of the dc component corresponding to progressive depolarisation in the TCR population. However, Fig. 3d show that the dominant alpha rhythmic region correspond to a mean output voltage of $\approx -70$ mV. The contour plots showing a distinct alpha peak in the region where $-32 \geqslant V_{thr} \geqslant -33$ and $3.7 \leqslant \sigma \leqslant 3.8$ (indicated by an arrow in Fig. 3c). Based on this observation, we set the base values for $V_{thr}$ and $\sigma$ to $-32$ mV and 3.7 mV respectively and study the alpha and theta rhythmic content in the model output.

### Alpha and Theta Band Power Variations

Figure 4 shows that the maximum power content with lower values of neurotransmitter concentration and higher mean membrane potential is primarily due to a high corresponding theta band power. Furthermore, the bar-plots show a left skew in the theta band power for progressively increasing values of $\sigma$, in contrast to a right-skew for the corresponding alpha band power. With progressively decreasing values of $V_{thr}$, the alpha band power shifts until for $-35 \geqslant V_{thr} \geqslant -38$, the maximum powers in both alpha and theta bands decrease exponentially with increasing values of $\sigma$. For $V_{thr} \leqslant -39$, the power in theta band falls significantly, and there is minimal effect on both bands for varying values of $\sigma$.

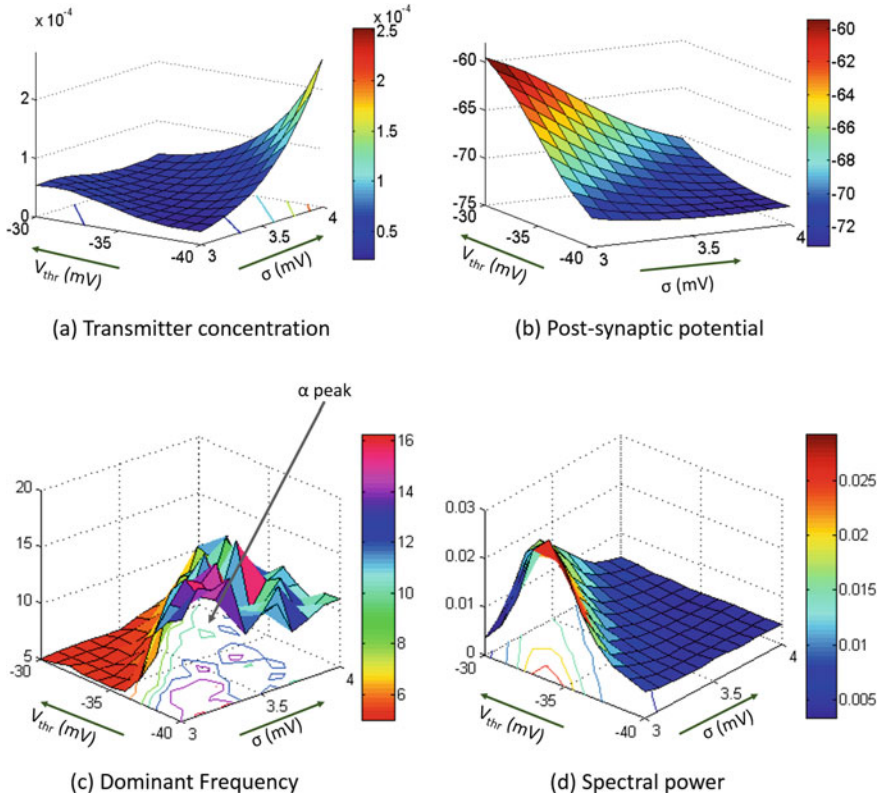


**Fig. 3** **a** The neurotransmitter concentration [$T$] with simultaneous variation of $V_{thr}$ (from −30 to −40 in steps of −1) and $\sigma$ (from 3 to 4 in steps of 0.1), and **b** the corresponding effect on the average population post-synaptic membrane potential $V_{TCR}$. The corresponding **c** dominant frequency of oscillation show specific regions of alpha and theta band dominance, while **d** the power in the frequency spectra indicate a high power within the theta band for lower values of the steepness parameter $\sigma$. It is worth reminding the readers at this point (see Fig. 1 legend) that the parameters $V_{thr}$ and $\sigma$ are set as equal for both AMPA or $GABA_A$ mediated synapses. Thus, any variation of these parameters will result in a variation of neurotransmitter concentration in all the synaptic clefts in the model, thus simulating conditions of an overall reduction in synaptic activity in the model

## *Role of the Thalamic Interneurons*

Neural mass models of the thalamocortical circuitry has been simulated traditionally with two neural populations viz. the TCR and the TRN [12, 57]. These models were intended to simulate brain rhythm alterations and abnormal oscillations corresponding to disease conditions. Several of these studies have demonstrated that the feed-forward and -back connections between the TCR and the TRN can well mimic the dynamics of several disease conditions for example bifurcation of EEG time-series seen in epilepsy [13, 35, 58, 67, 69, 72, 73], EEG anomalies in Alzheimer's

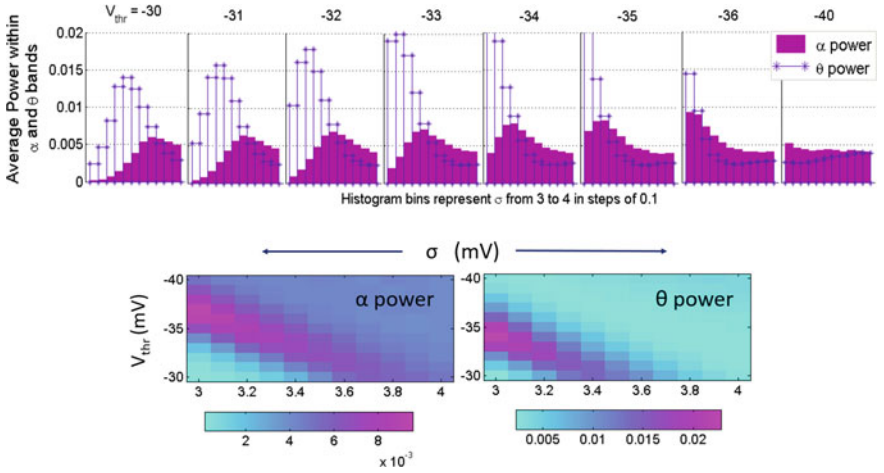


**Fig. 4** (*Top*) Bar plots showing the relative distribution of alpha and theta band power in the model output with varying values of $V_{thr}$ and $\sigma$. (*Bottom*) A 2-d representation to demonstrate the complementary pattern of dominance between the alpha and theta bands

disease [7, 16, 27], sleep-wake transition [1]. However, experimental studies indicate the presence of the IN cells in the LGN across mammals and rodents, comprising 20–25 % of the total cell population in the LGN and receive around 47 % of their total synaptic inputs from the retinal spiking neurons. Along these lines, further experimental investigation into the specific role of IN cells in the LGN may be suggested [17].

In section "The Causality of Neurotransmitter Concentration", we have tuned the neurotransmitter concentration parameters so that the model output oscillates with a dominant frequency within the alpha band. The time-series and power spectral density of all three cell populations are shown in Fig. 5 panels (a) and (c) respectively. The TCR and IN peak-to-peak oscillation is ≈1 mV; the same for TRN, however, is suppressed and is in the range of a few $\mu V$. The mean membrane potential of both the inhibitory populations viz. IN and TRN are greater than that of the TCR population. The power spectra indicates dominant power within the alpha band for both IN and TCR cell populations, while the dominant frequency of oscillation for the TRN is within the theta band.

Next, we remove the IN from the circuit to observe the output behaviour when all parameters are maintained at their respective base values. The time-series and power spectral density are shown in Fig. 5 panels (b) and (d) respectively. The TCR and TRN outputs show synchronised spindle oscillations with a dominant frequency at ≈11 Hz and within the alpha band. The amplitude of peak-to-peak oscillations is also increased in both TCR and TRN at ≈1.5 mV.

These observations may indicate a vital role of the IN in waking state EEG dynamics. Alpha rhythmic waxing-and-waning high amplitude oscillations are EEG markers of quiet wakefulness with eyes closed i.e. absence of sensory inputs, while alpha

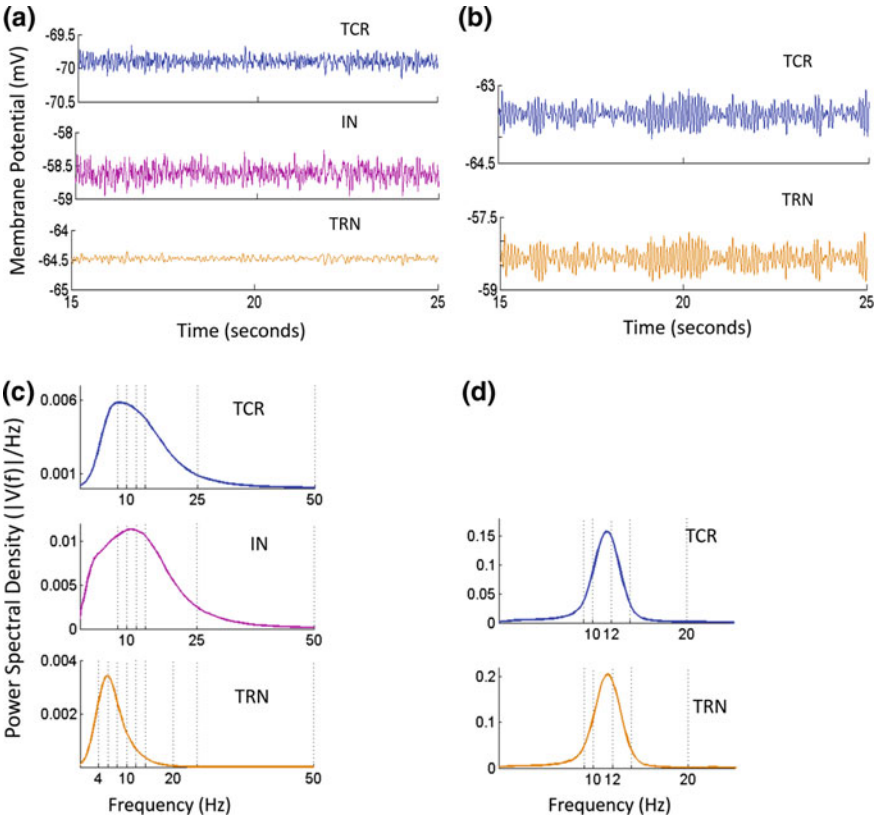


**Fig. 5** **a** Time-series output of the thalamic cell populations in the model when all parameters are set at their base values as indicated in Tables 1 and 2. The corresponding power spectra in (**c**) indicate a dominant alpha rhythmic oscillation in the TCR and IN population output, while the TRN oscillates with a dominant frequency within the theta band. **b** The time-series output of TCR and TRN when the IN is disconnected from the circuit by setting the synaptic connectivity parameter $C_{tii} = 0$ (refer to Table 2). High amplitude synchronised oscillations is observed in both TCR and TRN populations. The corresponding power spectra in (**d**) indicate a sharp alpha peak at around 11.5 Hz for both TCR and TRN

rhythmic noisy oscillations are now known to be important indicators of several cognitive brain states. Thus, the model predicts specific role for each inhibitory cell population in the thalamic circuitry: the TRN assumes prominence during wake to sleep transition and in sleep states, while the IN dominates the inhibitory influence on TCR during the waking state. In the context of neurological disorders, the IN may play a role in maintaining homeostasis, while any anomaly in this circuitry may trigger an onset of abnormal high amplitude synchronous oscillations in the TCR and TRN.

## *Effects of the Leak Conductance*

Anaesthetics are known to decrease excitability in muscles by increasing membrane leakage conductance. Furthermore, literature review of both experimental and modelling studies show evidence of the role of potassium leak channels in depolarisation/hyperpolarisation of population membrane potentials [34]. In addition, acetylcholine is known to cause hyperpolarisation in IN cells by increasing membrane potassium conductance. These results motivated us to investigate the effects of membrane leakage conductance in the model on its output.

To test the effect of increased leak conductance in our model, $g^{leak}$ for any one cell population is increased to 100 progressively, while the values of the same for the other two cell populations remain at their base values of 10.

When $g^{leak} = 100$ for the TCR population, both TCR and TRN population are depolarised, and removing the IN did not show any drastic change in the output characteristics.

When $g^{leak} = 100$ for the IN population, their mean membrane potential is hyperpolarised, causing a reduced effect on TCR and TRN populations, both of which show a depolarisation. This is similar to the case in section "Role of the Thalamic Interneurons" when the IN population is removed from the circuit.

When $g^{leak} = 100$ for the TRN population, their mean membrane potential is hyperpolarised and the TCR population is depolarised as shown in Fig. 6b (compare with Fig. 6a corresponding to base parameter values). However, if the IN is removed

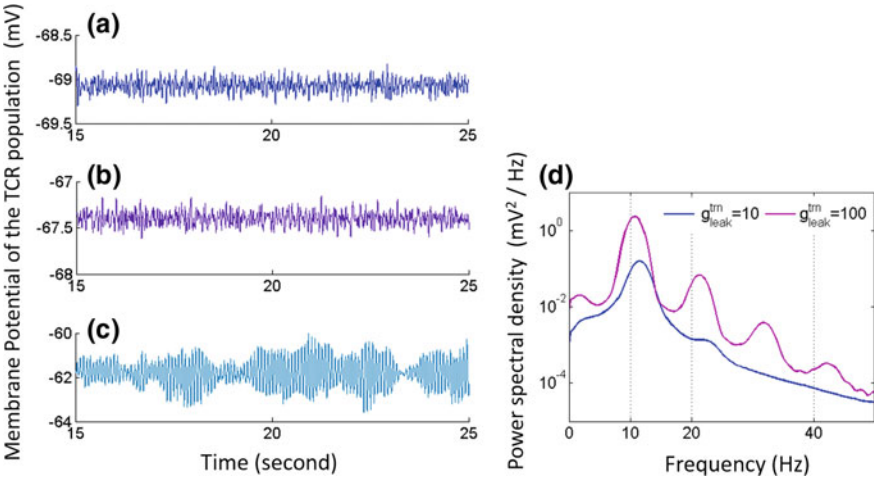


**Fig. 6** The model output time-series corresponding to **a** base parameter values of $g^{leak}$ for all cell populations in the model; **b** $g^{leak} = 100$ for TRN population and $g^{leak} = 10$ for TCR and IN; **c** $g^{leak} = 100$ for TRN and IN is removed from the circuit, while $g^{leak} = 10$ for TCR. **d** The power spectral density of the output obtained in (**c**) show a peak frequency within the alpha with harmonics (*violet*). A comparison is made with the power spectra for when $g^{leak} = 10$ (*blue*)

from the circuit, increasing $g^{leak}$ for the TRN population cause a depolarisation in both TRN and TCR populations. The time-series of both cell populations show a bifurcation to high amplitude oscillations shown in Fig. 6c, while the power spectral plot in Fig. 6d shows harmonics of the dominant frequencies within the alpha band. A comparison with the power spectra when all parameters are at base values, i.e. $g^{leak} = 10$ for all populations, and IN is removed from the circuit, is also shown for the convenience of readers.

In summary, these results show that for a model of the LGN tuned to oscillate within the alpha band, an increase of leak conductance in the inhibitory cell populations, IN or TRN, will lead to a depolarisation of the excitatory TCR cell population for normal neurotransmitter concentration levels, thus conforming to experimental evidence [34]. However, if the influence of IN is reduced while leak conductance of TRN is increased, both TCR and TRN are depolarised leading to bifurcation of the time-series to a high amplitude limit cycle oscillations with harmonics in the power spectra. Once again, the results imply a role of the IN in maintaining an overall system stability.

In the following section, we summarise the results and outline future research directions.

## Conclusion

We have presented a novel neural mass modelling approach to link the attributes of neuronal chemical synapses to higher level brain dynamics observed in Electroencephalogram (EEG) and Local Field Potential (LFP); this is done by replacing the traditional 'alpha function', which are used to model neuronal synaptic information transfer, with kinetic models of AMPA (excitatory) and $GABA_A$ (inhibitory) neuroreceptor mediated synapses. The paradigm was introduced to neuro-computational modelling in [26]. Subsequently, kinetic model of $GABA_A$-ergic synapse has been implemented in a single neuronal network model of the hippocampal circuit towards novel neuro-pharmacological paradigms and possible application in drug discovery [30]. In prior works, we have used neural mass models embedded with 'two-state' (open and closed states of ion channels; the desensitised state is ignored for brevity) kinetic models of synaptic transmission to study brain state transitions and the underlying cellular mechanisms [5]. Our study showed that replacing the alpha function with kinetic models of synapses improved the computational time of model simulation by a factor of 10 in comparison to the 'classic' neural mass modelling framework. In this chapter, we have built on these prior works and investigated the underlying neuronal correlates of alpha (8–13 Hz) and theta (4–7 Hz) EEG rhythms that are useful biomarkers in several neurological and psychiatric disorders.

Experimental evidence suggest that similar thalamic mechanisms underline alpha and theta rhythms, and that the thalamus is a key player in thalamocortical generation of these rhythms. This is not surprising as thalamocortical dysrhythmia (TCD) is a known feature in neurological disorders such as Depressive disorders,

Neurogenic Pain, Parkinson's disease, Tinnitus, Alzheimer's disease. On the other hand, transition from alpha to theta rhythm in a healthy, adult brain corresponds to brain state transition from quiet wakefulness (dominant alpha rhythm) to that of drowsiness (dominant theta rhythm). Thus, a computational model-based study to underpin the synaptic correlates of alpha and theta rhythms seems appropriate and useful in current times.

The model in this work emulates the neuronal populations of the Lateral Geniculate Nucleus (LGN), the thalamic nucleus in the visual pathway of mammals and rodents, and the intra-population synaptic connectivity mediated by AMPA and $GABA_A$ neuroreceptors. Please refer to Fig. 2 in the text for a schematic of the model consisting of the thalamocortical relay (TCR) cells that are the main carriers of sensory information from the retina to the visual cortex, the inhibitory interneurons (IN) that constitute around 20–25 % of the cells in the LGN, and the thalamic reticular nucleus (TRN), which is a thin sheet of inhibitory cell populations that are considered a part of the thalamus and receives 'copies' of all efferent and afferent communications between the thalamus and the cortex. The model input is a random noise with a white power spectrum, and may be thought to emulate the background firing activity of retinal ganglion cells under conditions of eyes closed i.e. no sensory input, and when the subject is in an awake but resting state, often referred to as a state of 'quiet wakefulness'. Both EEG and LFP recordings in quiet wakefulness, for example in the stage preceding sleep, indicate a strong alpha rhythmic content. Furthermore, simultaneous EEG recordings from the occipital scalp electrode (the seat of visual cortex) and LFP recordings from the TCR cells show a high coherence in their time-series. Thus, the output of the TCR cell population in the model is considered as the 'model output'.

Traditionally, neural mass models of the thalamocortical circuitry have explored the rich dynamics of the feed-forward and -back loop between the TCR and TRN that can emulate time-series and frequency domain behaviour of several neurological and psychiatric disorders. Thus, the IN cells have largely been ignored, in spite receiving around 47 % of their afferents from the retinal spiking neurons. This may be due to lack of experimental data on the IN characteristics, which in turn is attributed to insufficient technological advances. In this scenario, a computational model seems to be an apt tool to make investigations into the IN and its role in the thalamocortical dynamics. Towards this, a simple test is adopted by disconnecting the IN population from the circuitry. Indeed the time-series of both TRN and TCR are synchronised with a high magnitude of oscillation. Furthermore, waxing-and-waning patterns are observed and the power spectra indicates the dominant alpha rhythmic content with a peak at around 11.5 Hz. This result is consistent with several other prior work on the classic neural mass model of the thalamocortical circuitry consisting of just the TCR and TRN cell populations. Next, the IN is re-connected to the circuitry. The time-series output of the TCR changes significantly with a noisy pattern and low average amplitude reflecting the noisy input to the model, and a peak frequency within the alpha band; the time-series of the IN has a similar characteristic, albeit with a broader power spectral density peak within the alpha frequency band. The TRN output undergoes a remarkable change and appears to be suppressed by the dominant inhibitory

influence of the IN on the TCR, and its peak frequency of oscillation is ≈6 Hz within the theta frequency band. Thus, the model predicts a significant influence of the IN on the TRN in spite an absence of direct synaptic contact between the two populations. The results raise the speculation that in a healthy adult brain, the IN plays a dominant role in modulating TCR response in awake cognitive states; the diminished activity of IN in a quiet resting brain state establishes the dominant inhibitory influence of TRN on the TCR, leading to high amplitude synchronous oscillations. These observations call for further experimental research correlating the role of IN in higher level brain dynamics.

Another attribute that has received relatively reduced attention in computational modelling of neurological disorders, albeit with a few exceptions e.g. [29, 30], is the neurotransmitter concentration in synaptic clefts. Once again, the model presented here facilitates such a research direction. The neurotransmitter concentration in the synaptic cleft (refer to Eq. 2 in section "AMPA and $GABA_A$ Based Neurotransmission") is simulated with a sigmoid function that is sensitive to (a) the threshold voltage at which the neurotransmitter concentration is half the maximum value, as well as to (b) the steepness parameter of the sigmoid that indicates the proportionality of the amount of transmitter released to the pre-synaptic membrane potential. Our results show that an increase in the neurotransmitter concentration in the synaptic cleft is effected by a decrease in the threshold pre-synaptic membrane voltage, which agrees to an intuitive understanding of the phenomenon. However, the neurotransmitter concentration is also increased by a decrease in the steepness of the sigmoid. From a systems perspective, the phenomenon can be explained thus: for a steep sigmoid, the neurotransmitter concentration reaches saturation ($\approx T_{max}$) or 'cut off' ($\approx 0$) for low-range fluctuation of the pre-synaptic voltage about the threshold voltage. Thus, the neurotransmitter concentration follows a spike train-like all-or-none pattern, which effectively reduces the average value of the parameter. On the other hand, with lesser steepness, the 'operating region' of the sigmoid is much larger prior to the concentration reaching either saturation or cut-off, thus effecting higher average concentration levels in the synaptic cleft.

In terms of frequency domain response with varying neurotransmitter concentrations, we note an interesting complementary behaviour in the alpha and theta band power content. With lower neurotransmitter concentration levels in the circuit, the theta band dominates and with an overall higher magnitude of power in the spectra. Peak alpha band power is observed when neurotransmitter concentration is at a mid-range value. This may also be interpreted as a shift from alpha to theta band power for raised threshold pre-synaptic membrane potential and steepness values for the neurotransmitter release/concentration, and may reflect abnormalities of chemical synaptic attributes corresponding to TCD. It may be noted that in the current work, we have considered simultaneous changes in the neurotransmitter concentration in all synaptic clefts in the model; the objective has been to study a more holistic effect of fluctuations in synaptic activity in the system. For example during transition from wakefulness to sleep, it may be speculated, intuitively, that there is a change in overall system behaviour leading to high-amplitude low-frequency synchronous oscillations across larger brain areas. However, this needs further investigation with

distinct neurotransmitter concentration for each synaptic cleft in the model. Furthermore, a dynamic adaptability in this attribute may be desirable when investigating specific disease conditions; these directions are planned as future work on the model.

A preliminary observation on the effects of leakage conductance in the model re-iterates the prominent role of IN over TCR in normal brain states, maintaining an overall homeostasis in the circuit. Recent research proposes a possible role of potassium leakage currents in epileptic seizures [33], while potassium leak currents are known to affect cell response by causing de-(hyper-)polarisation in cell membrane potentials. Also, the effects of anaesthetics in decreasing muscle excitability is facilitated by increasing population leakage conductance. In the model, increasing the leakage conductance of both IN and TRN populations cause a depolarisation of the TCR cells. However, when the IN is disconnected from the circuit, an increase in leakage conductance in the TRN cells causes a bifurcation in the TCR output leading to high amplitude limit-cycle like oscillations with slight waxing and waning envelope modulation. Frequency analysis shows alpha band dominance. It may be noted that theta band limit cycles are seen with decreased neurotransmitter concentrations under these conditions. Once again, the results indicate an overall homeostatic role of the IN in the LGN circuitry and conforming to a healthy, awake and cognitive brain state. Disruption in factors affecting homeostasis in the brain is implicated in several disease conditions. The model-based observations in this work implicates disruption of the IN circuitry as a possible underlying factor for certain disease related homeostatic abnormalities that reflect in higher level brain dynamics recorded via EEG and LFP.

It is worth mentioning here that in a similar work on the classic neural mass models, we have looked into synaptic connectivity parameters that effect a 'slowing' (left-shift of peak frequency of oscillation) of the alpha rhythm, a definite biomarker of Alzheimer's disease [8]. However, investigation into further synaptic attributes has not been possible due to model limitations on detailed synaptic attributes; in comparison, the modified neural mass modelling approach presented in this work have alleviated this constraint to a fair extent. However, several levels of abstraction are adopted in the model for brevity—first, the $GABA_B$ pathway from the TRN to the TCR is ignored; second, the kinetic models of the synapses are two-state models i.e. the desensitised state is not considered here; third, feedback from the TCR to the IN is ambiguous in literature, and thus are not explored in this work; fourth, the neurotransmitter concentration in synaptic clefts has similar parameters for all cell populations (afore-mentioned in this section); fifth, while the present model aims to underpin the rhythmic behaviour of the LGN when de-corticated, i.e. disconnected from the visual cortex, however, cortico-thalamic feedback is an integral factor in the generation and sustenance of brain rhythms observed in EEG. All of these abstractions will be looked into in a future work.

Ongoing research is looking into implementing a neural mass cortical circuitry that will then be linked to the LGN model presented in this work. While such a model has already been explored in a prior work, the novelty will be the introduction of synaptic kinetics in such a thalamo-cortico-thalamic neural mass framework. Furthermore, a recent research has used the classic alpha rhythm neural mass

model to emulate EEG signals corresponding to trains of flickering visual stimuli, commonly termed as steady-state-visually-evoked-potentials; the model results were validated with experimental data [47]. Using computational models to emulate steady-state-visually-evoked-potentials was initiated in [59]; the potential of the neural mass framework presented herewith will be tested along these lines.

Overall, the study presented herewith have contributed in justifying the ongoing endeavours to build biologically-inspired computational paradigms that are computationally efficient and can contribute to progressing the diagnosis, prognosis and prediction of neurological and psychiatric disorders. The observations made in this work call for further experimental data for the purposes of model validation and continued advancement of research in computational neurology and neuropsychiatry.

**Acknowledgements** The authors would like to acknowledge the contribution of Vincent N. Martin, second year undergraduate student of Mechanical Engineering at the University of Lincoln, for his contributions to Fig. 3 in this work as a part of his coursework. We thank the reviewers for very useful suggestions towards improving the manuscript. BSB is grateful to Piotr Suffczynski for useful discussions on the model during his visit to the University of Lincoln (July-September 2015) supported by DVF1415/2/35 grant, awarded by the Royal Academy of Engineering, UK.

## References

1. Abeysuriya, R., Rennie, C., Robinson, P.: Prediction and verification of nonlinear sleep spindle. Journal of Theoretical Biology **344**, 70–77 (2014)
2. Aradi, I., Érdi, P.: Computational neuropharmacology: dynamical approachers in drug discovery. TRENDS in Pharmacological Sciences **27**(5), 240–243 (2006)
3. Bal, T., von Krosigk, M., McCormick, D.A.: Synaptic and membrane mechanisms underlying synchronized oscillations in the ferret lateral geniculate nucleus *in vitro*. Journal of Physiology **483**, 641–663 (1995)
4. Bernard, C., Ge, Y., Stockley, E., Willis, J., Wheal, H.: Synaptic integration of NMDA and non-NMDA receptors in large neuronal network models solved by means of differential equations. Biological Cybernetics **70**, 267–273 (1994)
5. Bhattacharya, B.S.: Implementing the cellular mechanisms of synaptic transmission in a neural mass model of the thalamo-cortico circuitry. Frontiers in Computational Neuroscience **81**, 1–11 (2013)
6. Bhattacharya, B.S., Chowdhury, F.N. (eds.): Validating neuro-computational models of neurological and psychiatric disorders, *Springer series in Computational Neuroscience*, vol. 14. Springer (2015)
7. Bhattacharya, B.S., Coyle, D., Maguire, L.P.: Thalamocortical circuitry and alpha rhythm slowing: an empirical study based on a classic computational model. In: Proceedings of the International Joint Conference on Neural Networks (IJCNN), pp. 3912–3918. Barcelona, Spain (2010)
8. Bhattacharya, B.S., Coyle, D., Maguire, L.P.: Alpha and theta rhythm abnormality in Alzheimer's disease: a study using a computational model. In: C. Hernandez, J. Gomez, R. Sanz, I. Alexander, L. Smith, A. Hussain, A. Chella (eds.) Advances in Experimental Medicine and Biology, Volume 718, pp. 57–73. Springer New York (2011)
9. Bhattacharya, B.S., Coyle, D., Maguire, L.P.: A thalamo-cortico-thalamic neural mass model to study alpha rhythms in Alzheimer's disease. Neural Networks **24**, 631–645 (2011)
10. Bhattacharya, B.S., Coyle, D., Maguire, L.P., Stewart, J.: Kinetic modelling of synaptic functions in the alpha rhythm neural mass model. In: A.V. et al (ed.) ICANN 2012 Part I, Lecture Notes in Computer Science 7552, pp. 645–652. Springer Verlag Berlin Heidelberg (2012)

11. Bond, T., Durrant, S., O'Hare, L., Turner, D., Bhattacharya, B.S.: Studying the effects of thalamic interneurons in a thalamocortical neural mass model. In: BMC Neuroscience (Suppl 1), vol. 15, p. P219 (2014)
12. Breakspear, M., Roberts, J., Terry, J., Rodrigues, S., Mahant, N., Robinson, P.A.: A unifying explanation of primary generalized seizures through nonlinear brain modelling and bifurcation analysis. Cerebral Cortex **16**, 1296–1313 (2006)
13. Breakspear, M., Terry, J.R., Friston, K.J.: Modulation of excitatory synaptic coupling facilitates synchronization and complex dynamics in a nonlinear model of neuronal dynamics. Neurocomputing **52**, 151–158 (2003)
14. Buzsáki, G.: Rhythms of the Brain, first edn. Oxford University Press, New York (2006)
15. Carta, M., Lanore, F., Rebola, N., Szabo, Z., da Silva, S.V., Lourenco, J., Verraes, A., Nadler, A., Schultz, C., Blanchet, C., Mulle, C.: Membrane lipids tune synaptic transmission by direct modulation of presynaptic potassium channels. Neuron **81**(4), 787–799 (2014)
16. Coyle, D., Bhattacharya, B.S., Zou, X., Wong-Lin, K., Abuhassan, K., Maguire, L.: Neural circuit models and neuropathological oscillations. In: N. Kasabov (ed.) Handbook of Bio-Neuro-Informatics, pp. 673–702. Springer (2014)
17. Crunelli, V., Cope, D.W., Hughes, S.W.: Thalamic t-type calcium channels and nrem sleep. Cell Calcium **40**, 175–190 (2006)
18. Crunelli, V., Haby, M., Jassik-Gerschenfeld, D., Leresche, N., Pirchio, M.: $Cl^-$-and $k^+$-dependent inhibitory postsynaptic potentials evoked by interneurons of the rat lateral geniculate nucleus. Journal of Physiology **399**, 153–176 (1988)
19. daSilva, F.H.L., Hoeks, A., Smits, H., Zetterberg, L.H.: Model of brain rhythmic activity. Kybernetic **15**, 27–37 (1974)
20. daSilva, F.H.L., van Lierop, T.H., Schrijer, C.F., van Leeuwen, W.S.: Organisation of thalamic and cortical alpha rhythms: spectra and coherences. Electroencephalography and Clinical Neurophysiology **35**, 627–639 (1973)
21. David, O., Friston, K.J.: A neural mass model for MEG/EEG: coupling and neuronal dynamics. NeuroImage **20**, 1743–1755 (2003)
22. Deco, G., Jirsa, V.K., Robinson, P.A., Breakspear, M., Friston, K.: The dynamic brain: from spiking neurons to neural masses and cortical fields. PLOS Computational Biology **4**(8), e1000,092 (2008)
23. Destexhe, A.: Synthesis of models for excitable membranes, synaptic transmission and neuromodulation using a common kinetic formalism. Journal of Computational Neuroscience **1**, 195–230 (1994)
24. Destexhe, A., Mainen, Z., Sejnowski, T.: An efficient method for computing synaptic conductances based on a kinetic model of receptor binding. Neural Computation **6**, 14–18 (1994)
25. Destexhe, A., Mainen, Z., Sejnowski, T.: Kinetic models of synaptic transmission. In: C. Koch, I. Segev (eds.) Methods in neuronal modelling, pp. 1–25. MIT Press, Cambridge, MA (1998)
26. Destexhe, A., Mainen, Z., Sejnowski, T.: Kinetic models for synaptic interactions. In: M. Arbib (ed.) The handbook of brain theory and neural networks, pp. 1126–1130. MIT Press, Cambridge, MA (2002)
27. de Haan, W., Mott, K., van Straaten, E.C.W., Scheltens, P., Stam, C.J.: Activity dependent degeneration explains hub vulnerability in Alzheimer's disease. PLOS Computational Biology **8**(8), e100,252 (2012)
28. Dodson, P.D., Forsythe, I.D.: Presynaptic k+ channels: electrifying regulators of synaptic terminal excitability. Trends in Neurosciences **27**(4), 210–217 (2004)
29. Érdi, P., John, T., Kiss, T., Lever, C.: Discovery and validation of biomarkers based on computational models of normal and pathological hippocampal rhythms. In: B.S. Bhattacharya, F.N. Chowdhury (eds.) Validating neuro-computational models of neurological and psychiatric disorders, pp. 15–42. Springer (2015)
30. Érdi, P., Kiss, T., Tóth, J., Ujfalussy, B., Zalányi, L.: From systems biology to dynamical neuropharmacology: proposal for a new methodology. IEEE Proceedings of Systems Biology **153**(4), 299–308 (2006)

31. Francis, P.T., Palmer, A.M., Snape, M., Wilcock, G.K.: The cholinergic hypothesis of alzheimer's disease: a review of progress. Journal of Neurology and Neurosurgical Psychiatry **66**(2), 137–147 (1999)
32. Freeman, W.J.: Mass action in the nervous system, first edn. Academic Press, New York (1975)
33. Gentiletti, D., Gnatkovsky, V., de Curtis, M., Suffczyński, P.: Changes of ionic concentrations during seizure transitions - a modeling study. Under Review (2016)
34. Goldstein, S., adn Ita O'Kelly, D.B., Zilberberg, N.: Potassium leak channels and the kcnk family of two-p-domain subunits. Nature Reviews Neuroscience **2**, 175–184 (2001)
35. Golomb, D., Wang, X.J., Rinzel, J.: Synchronization properties of spindle oscillations in a thalamic reticular nucleus model. Journal of Neurophysiology **72**(3), 1109–1126 (1994)
36. Golomb, D., Wang, X.J., Rinzel, J.: Propagation of spindle waves in a thalamic slice model. Journal of Neurophysiology **75**, 750–769 (1996)
37. Grimbert, F., Faugeras, O.: Bifurcation analysis of Jansen's neural mass model. Neural Computation **18**, 3052–3068 (2006)
38. Guillery, R.W., Sherman, S.M.: The thalamus as a monitor of motor outputs. Philosophical Transactions of the Royal Society of London B Biological Science **357**(1428), 1809–1821 (2002)
39. Harris, K.P., Littleton, J.T.: Transmission, development and plasticity of synapses. Genetics **210**(2), 345–375 (2015)
40. Horn, S.C.V., Erisir, A., Sherman, S.M.: Relative distribution of synapses in the A-laminae of the lateral geniculate nucleus of the cat. The Journal of Comparative Neurology **416**, 509–520 (2000)
41. Hughes, S.W., Crunelli, V.: Thalamic mechanisms of eeg alpha rhythms and their pathological implications. The Neuroscientist **11**(4), 357–372 (2005)
42. Hughes, S.W., Lorincz, M., Cope, D.W., Blethyn, K.L., Kekesi, K.A., Parri, H.R., Juhasz, G., Crunelli, V.: Synchronised oscillations at $\alpha$ and $\theta$ frequencies in the lateral geniculate nucleus. Neuron **42**, 253–268 (2004)
43. Jansen, B.H., Rit, V.G.: Electroencephalogram and visual evoked potential generation in a mathematical model of coupled cortical columns. Biological Cybernetics **73**, 357–366 (1995)
44. Jeong, J.: Eeg dynamics in patients with alzheimer's disease. Clinical Neurophysiology **115**, 1490–1505 (2004)
45. Jones, E.G.: The Thalamus, Vol. I and II, first edn. Cambridge University Press, Cambridge, UK (2007)
46. von Krosigk, M., Bal, T., McCormick, D.A.: Cellular mechanisms of a synchronised oscillation in the thalamus. Science **261**, 361–364 (1993)
47. Labecki M, Kus R, Brzozowska A, Stacewicz T, Bhattacharya BS and Suffczynski P (2016). Nonlinear origin of SSVEP spectra–a combined experimental and modeling study. Front. Comput. Neurosci. 10:129. doi:10.3389/fncom.2016.00129
48. Liljenstrom, H.: Mesoscopic brain dynamics. Scholarpedia **7**(9), 4601 (2012)
49. Llinas, R., Urbano, F.J., Leznik, E., Ramirez, R.R., van Marle, H.J.: Rhythmic and dysrhythmic thalamocortical dynamics: Gaba systems and the edge effect. Trends in Neuroscience **28**(6), 325–333 (2005)
50. Lörincz, M.L., Crunelli, V., Hughes, S.W.: Cellular dynamics of cholinergically induced $\alpha$ (8–13 hz) rhythms in sensory thalamic nuclei *In Vitro*. The Journal of Neuroscience **628**(3), 660–671 (2008)
51. McCormick, D.A., Pape, H.C.: Properties of a hyperpolarization-activated cation current and its role in rhythmic oscillation in thalamic relay neurones. Journal of Physiology **431**, 291–318 (1990)
52. McCormick, D.A., Prince, D.A.: Actions of acetylcholine in the guinea-pig and cat medial and lateral geniculate nuclei, *In Vitro*. Journal of Physiology **392**, 147–165 (1987)
53. Modolo, J., Thomas, A., Legros, A.: Neural mass modelling of power-line magnetic fields effects on brain activity. Frontiers in computational neuroscience **7**, 34 (2013)
54. Moran, R., Pinotsis, D.A., Friston, K.: Neural masses and fields in dynamic causal modeling. Frontiers in Computational Neuroscience **7**, 1–12 (2013)

55. Pons, A.J., Cantero, J.L., Atienza, M., Garcia-Ojalvo, J.: Relating structural and functional anomalous connectivity in the ageing brain via neural mass modelling. NeuroImage **52**(3), 848–861 (2010)
56. Rall, W.: Distinguishing theoretical synaptic potentials computed for different soma-dendritic distributions of synaptic inputs. Journal of Neurophysiology **30**, 1138–1168 (1967)
57. Robinson, P., Phillips, A., Fulcher, B., Puckeridge, M., Roberts, J.: Quantitative modelling of sleep dynamics. Philosophical Transactions of the Royal Society A **369**, 3840–3854 (2011)
58. Robinson, P., Rennie, C., Rowe, D.: Dynamics of large-scale brain activity in normal arousal states and epileptic seizures. Physical Review E **65**, 041,924 (2002)
59. Robinson, P.A., Postnova, S., abeysuriya, R.G., Kim, J.W., Roberts, J.A., McKenzie-Sell, L., Karanjai, A., Kerr, C.C., fung, F., Anderson, R., Breakspear, M.J., Drysdale, P.M., Fulcher, B.D., Phillips, A.J.K., Rennie, C.J., Yin, G.: A multiscale "working brain" model. In: B.S. Bhattacharya, F.N. Chowdhury (eds.) Validating neuro-computational models of neurological and psychiatric disorders, pp. 107–140. Springer (2015)
60. Sarnthein, J., Morel, A., von Stein, A., Jeanmonod, D.: Thalamic theta field potentials and eeg: high thalamocortical coherence in patients with neurogenic pain, epilepsy and movement disorders. Thalamus and related systems **2**, 231–238 (2003)
61. Sherman, S.M.: Thalamus. Scholarpedia **1**(9), 1583 (2006)
62. Sherman, S.M., Guillery, R.W.: Exploring the thalamus, first edn. Academic Press, New York (2001)
63. Sotero, R.C., Tujillo-Barreto, N.J., Iturria-Medina, Y.: Realistically coupled neural mass models can generate EEG rhythms. Neural Computation **19**, 479–512 (2007)
64. Steriade, M., McCormick, D.A., Sejnowski, T.J.: Thalamocortical oscillations in the sleeping and aroused brain. Science **262**(5134), 679–685 (1993)
65. Steriade, M.M., McCarley, R.: Brain control of wakefulness and sleep, second edn. Kluwer Academic/Plenum Publishers, New York (2005)
66. Suffczyński, P.: Neural dynamics underlying brain thalamic oscillations investigated with computational models. Ph.D. thesis, Institute of experimental physics, University of Warsaw (2000)
67. Suffczyński, P., Kalitzin, S., Silva, F.L.D.: Dynamics of non-convulsive epileptic phenomena modelled by a bistable neuronal network. Neuroscience **126**, 467–484 (2004)
68. Taruno, A., Ohmori, H., Kuba, H.: Inhibition of pre-synaptic na(+)/k(+)-atpase reduces readily releasable pool size at the avian end-bulb of held synapse. Neuroscience Research **72**(2), 117–128 (2012)
69. Taylor, P.N., Wang, Y., Goodfellow, M., Dauwels, J., Moeller, F., Stephani, U., Baier, G.: A computational study of stimulus driven epileptic seizure abatement. PLOS one pp. 1–26 (2014)
70. Ursino, M., Cona, F., Zavaglia, M.: The generation of rhythms within a cortical region: Analysis of a neural mass model. NeuroImage **52**(3), 1080–1094 (2010)
71. Wang, X.J., Golomb, D., Rinzel, J.: Emergent spindle oscillations and intermittent burst firing in a thalamic model: specific neuronal mechanisms. Proceedings of the National Academy of Sciences **92**, 5577–5581 (1995)
72. Wang, X.J., Rinzel, J.: Alternating and synchronous rhythms in reciprocally inhibitory model neurons. Neural Computation **4**, 84–97 (1992)
73. Wang, Y., Goodfellow, M., Taylor, P.N., Baier, G.: Dynamic mechanisms of neocortical focal seizure onset. PLOS Computational Biology **10**(8), e1003,787 (2014)
74. Wendling, F., Bartolomei, F., Bellanger, J.J., Chauvel, P.: Epileptic fast activity can be explained by a model of impaired GABAergic dendritic inhibition. European Journal of Neuroscience **15**, 1499–1508 (2002)
75. Wilson, H.R., Cowan, J.D.: A mathematical theory of the functional dynamics of cortical and thalamic nervous tissue. Kybernetik **13**, 55–80 (1973)
76. Zetterberg, L.H., Kristiansson, L., Mossberg, K.: Performance of a model for a local neuron population. Biological Cybernetics **31**, 15–26 (1978)
77. Zhu, J.J., Lytton, W.W., Xue, J.T., Uhlrich, D.J.: An intrinsic oscillation in interneurons of the rat lateral geniculate nucleus. Journal of Neurophysiology **81**, 702–711 (1999)